Heat and Mass Transfer (2019) 55:3117–3131
https://doi.org/10.1007/s00231-019-02647-5

ORIGINAL

Research on heat transfer enhancement and flow characteristic of heat exchange surface in cosine style runner

Yongliang Zhang [1] · Xilong Zhang [1] · Min Li [1] · Zunmin Liu [1]

Received: 11 September 2018 / Accepted: 14 May 2019 / Published online: 27 May 2019

Abstract

The steady state heat transfer and flow resistance performance in cosine style runners with different amplitudes are studied numerically and experimentally in this paper. The results show that: When the Reynolds numbers (*Re*) range from 1210 to 5080, the core volume goodness factor ($\eta_o h_{std}\alpha$) is used to compare the overall heat transfer performance of the two runners, and the $\eta_o h_{std}\alpha$ value in the cosine style runner is 7–25% larger than that of the equal cross section runner, so that the cosine style runner has better overall heat transfer enhancement performance. When the amplitudes (2*A*) range from 5 to 9 mm, with the decrease of amplitude, the overall heat transfer performance is getting better. At the same amplitude, the convective heat transfer performance gradually increases as the inlet height (F_h) decreases; with the increase of *Re*, the thickness of the thermal and velocity boundary layers are both decreasing. Based on the field synergy principle, the heat transfer enhancement mechanisms with different parameters are evaluated, and we conclude that the smaller the amplitude is, its field synergy is better.

Nomenclature

A	Surface area [m^2]; Amplitude [mm]
c_p	Specific heat capacity [J/kg·K]
D_h	Hydraulic diameter [mm]
E	Fluid pumping power per unit surface area [W/m^2]
F_h	Inlet height [mm]
h	Heat transfer coefficient [$W/m^2·K$]
L_f	Fin length [mm]
ΔP	Pressure difference [Pa]
Q	Average value of the heat flux [W]
S_f	Fin pitch [mm]
T	Temperature [K]
t_f	Fin thickness [mm]
ΔT	Temperature difference [K]
u	Velocity [m/s]

Dimensionless

f	Fanning friction factor
g_c	Proportionality constant in Newton's second law of motion, $g_c = 1$
j	Colburn factor
Nu	Nusselt number
Pr	Prandtl number
Re	Reynolds number

Greek letters

α	Ratio of total heat transfer area to the total volume of an exchanger [m^2/m^3]
θ	Average field synergy angle [°]
θ'	Local field synergy angle [°]
ρ	Air density [kg/m^3]
λ	Heat conductivity [W/m·K]
μ	Dynamic viscosity [Pa·s]
η_o	Extended surface efficiency on one fluid side of the extended surface heat exchanger, dimensionless
σ	Ratio of free flow area to frontal area, dimensionless

Subscripts

A	Inlet air
B	Outlet air
C	Inlet water
D	Outlet water
in	Inlet
ln	Logarithm
m	Average value
max	Maximum value
w	Wall

✉ Xilong Zhang
beibitpap@hotmail.com

[1] School of Mechanical and Automotive Engineering, Qingdao University of Technology, Qingdao 266520, China

1 Introduction

So far, heat exchangers used in domestic and foreign are in the form of rectangular, circular or other regular equal cross

section heat exchange surface runner. However, while the cooling medium flows from the inlet to the outlet through the fins and the substrate of the equal cross section heat exchange surface runner, the temperature difference between inlet and the cooling medium has the largest value. The cooling medium is continuously heated while it flows to the outlet that resulting in a smaller temperature difference between the outlet and the cooling medium, which suppressing the ability of heat transfer from the substrate to the cooling medium in the downstream region of the runner [1]. In addition, the cooling medium generates a certain pressure loss during flowing, and the loss increases in the form of the quadratic with the increase of the flow rate, which greatly increased the consumption of the pump power and exacerbates the energy loss [2].

In view of the defects of the above-mentioned conventional equal cross section heat exchange surface runner, this paper presents a kind of cosine style heat exchange surface runner. The cosine style runner is a cosine-shaped structure with a gradually expanding shape on a section parallel to the flow direction. However, in the direction perpendicular to the flow, the shape of the cross-sectional area is rectangular, and the size of the cross-sectional area changes. The height and the heat transfer area of the fins gradually increase in the flowing process, so that more heat can be transferred. Thus the temperature difference between the fins and the cooling medium is relatively uniform, which enhances the capacity of convection heat transfer. Since the flow path is a diverged structure with big inlet and small outlet in the direction of flow, the cooling medium is also pressurized during the flow. Thus, the pressurizing process can greatly reduce the power consumption.

At present, the research on the runner of the cosine style heat exchanger has not been reported. But, there are many studies on trapezoidal tapered runner structure. Wu et al. [3] measured the friction coefficient in the trapezoidal cross section of smooth silicon-based microchannel with different hydraulic diameters. The Navier-Stokes equation is still valid when the hydraulic diameters range from 25.9 to 291.0 μm. Kuo et al. [4] numerically simulated the periodic trapezoidal structure and the method was used to evaluate the heat transfer performance and flow characteristics of the trapezoidal runner. They also found that the trapezoidal runner can reduce the field synergy angle between velocity vector and the temperature gradient, which can improve the field synergy in the runner. Amrahmadi et al. [5] used a vortex generator to analyze the forced convection heat transfer performance in a trapezoidal runner, and they solved the mass conservation, momentum and energy conservation equations by using finite volume method. For the trapezoidal runner structure in the above-mentioned references, the cross section perpendicular to the flow direction is a structure including rectangle, circle and trapezoid, while the equal section area remains unchanged. As for diverged flow path, there is little research on the trapezoidal tapered structure. For this kind of structure, Farhanieh et al. [6] studied the cross section of trapezoidal runner with different geometries by means of numerical analysis, and analyzed its flow and heat transfer performance in laminar flow. Li et al. [7] experimentally investigated the heat transfer performance of the trapezoidal runner inside the turbine blade under both rotating and static conditions. Zhang et al. [1] studied the flow and heat transfer characteristics in the trapezoidal heat exchange surface channel in laminar runner. The results showed that the temperature difference distribution in the trapezoidal runner was more uniform, and the pressure drop loss was lower than that of the equal cross section runner with the Reynolds numbers ranged from 800 to 3000. In contrast, with the same heat transfer area, the heat transfer factor and friction factor ratio of the trapezoidal runner increased by 8 and 22.6% respectively. At the same time, when the inclination angle of the trapezoidal runner is less than 40°, the overall heat transfer performance in the trapezoidal runner was better than the equal cross section runner.

In the application of trapezoidal flow path, Cur and Anselmino [8] first proposed an Accelerated Flow Evaporator which can replace common evaporator and reduce the volume, weight and manufacturing cost of evaporator. In the evaporator, the air was gradually accelerated by the contracted structure, thereby increased the local convection heat transfer performance of the downstream region. As a consequence, the increment of convection heat transfer can compensate the influence caused by the reduction of heat transfer area. However, the accelerated flow evaporator also increased reversible and irreversible pressure drop losses. The reversible pressure drop loss caused by the decreased heat transfer area in the downstream, but the irreversible pressure drop losses caused by the increased average velocity in downstream zone. Waltrich et al. [9–11] had also experimentally studied for this accelerated flow evaporator.

In addition to the trapezoidal runner structure, Rush et al. [12] studied the local heat transfer and flow characteristics in the sinusoidal corrugated runner under laminar and transitional flow conditions. They found that relatively significant flow instability exists at the outlet with small Reynolds numbers, and the unstable state gradually goes to the inlet as the Reynolds number increases. Akbarzadeh et al. [13–16] analyzed the sensitivity of heat transfer and pump work of nanofluids in corrugated runners. The mass, momentum and energy conservation equations of two-dimensional steady state were solved by finite volume method. It was found that the mixability of the fluid can be improved in the corrugated runner, and the temperature gradient at the wall surface increased with the increase of the amplitude. Ramgodia et al. [17] simulated three-dimensional numerical simulation of three corrugated runners with different phase angles, and analyzed the heat transfer and flow characteristics of fluid at different phase angles during the complete development phase. Bahaidarah et al. [18] studied the volumetric entropy production

rate in the corrugated runner. The results showed that the total entropy increases with the increase of *Re*. However, when the Reynolds numbers range from 25 to 400, the total entropy increase in the direction of the flow path is gradually reduced. Akbarzadeh et al. [19] also used entropy-increasing method to study three different types of special-shaped runners including sinusoidal, trapezoidal and triangular, and numerical simulation was carried out. The results for the three different structures showed that the sinusoidal structure has the best heat transfer performance. Sarkar et al. [20] investigated two-dimensional flow characteristics in corrugated runners at different Reynolds numbers ($100 < Re < 2123$). The heat transfer and flow properties of six structures under different amplitudes (0.05, 0.075 and 0.1 mm) and wavelength (0.5 and 1 mm) were investigated in the state of laminar flow and transition flow.

As can be seen from the analysis of the above mentioned references, the flow and heat transfer characteristics of the cosine type heat exchange surface runner structure are studied for the first time in this paper. The temperature field, flow field and synergy field of different cosine type structural parameters are experimentally and numerically studied. The cosine style runner can obviously improve the efficiency of the heat transfer and reduce the pressure drop.

2 Test study

2.1 Test sample

The effect of different cosine style runner parameters on heat transfer and pressure drop characteristics was studied by using orthogonal design method. The material used in the experiment was 6063 aluminum alloy, and the meridian cutting process was processed. In the process of experiment and simulation, the cosine curve with half wavelength ([0, π]) as the heat exchange surface of the runner. The divergent curved surface is also more conducive to discharge condensate [21].

The diagram of the cosine style runner structure is shown in Fig. 1. The equation of the cosine curve is $y = A \cdot cos(Bx)$, where $B = \pi / L_f$. Detailed dimension parameters of the cosine runner structure is shown in Table 1 including nine different experimental samples. As a reference runner of equal cross section, the picture of real product and schematic diagram of structural parameters are shown in Fig. 2a and b respectively. Tables 1 and 2 are specific structural parameters of the cosine style runner and equal cross section runner respectively.

2.2 Test bed

The schematic diagram of the test bed is shown in Fig. 3, which including an air circulation system, a water circulation system, a control system, a data acquisition system and other auxiliary systems. The measuring range and precision of air were 0.05–30 m/s and ± 5% respectively. A pulsed flow transducer was used to measure the water flow rate, which had an accuracy of 0.1 g. The JM9 compensation micro-manometer with higher precision is selected, which had the accuracy of 0.1 Pa. T-type thermocouple was used to measure temperature ranges from −200 to 300 °C, and its accuracy was ±0.1 °C.

The uncertainty in the experiment was analyzed according to the method proposed by Moffat [22]. The maximum uncertainty of convective heat transfer coefficient calculated by this method was 2.9%, and the maximum uncertainty of pressure drop ΔP was 5.1%. Therefore, the error of the system can meet the requirements of the experiment, and the experimental data had certain reliability. At the same time, each data point was obtained through three repeated measurements, and each measurement was maintained at a thermal equilibrium state for a minimum of 1 h.

2.3 Data processing method

The heat transfer coefficient (h) of air side can be expressed as:

$$h = \frac{Q}{A\Delta T_{\ln}} \tag{1}$$

where Q is the average value of the heat flux of air side and water side, $\Delta T_{\ln}$ is the logarithmic average temperature difference which can be described by [23]:

$$\Delta T_{\ln} = \frac{(T_C - T_B) - (T_D - T_A)}{\ln\left(\frac{T_C - T_B}{T_D - T_A}\right)} \tag{2}$$

The flow state of the fluid can be expressed in two Reynolds numbers according to a given fin and flow path structure. Two Reynolds numbers are used in the two types of runners, which are Re_{m} and $Re_{\max}$ respectively.

Reynolds number in the rectangular flow path is Reynolds number Re_{m}:

$$Re_m = \frac{u_m d_h}{\mu / \rho} \tag{3}$$

The flow condition of cosine runner can be evaluated by the maximum Reynolds number ($Re_{\max}$):

$$Re_{\max} = \frac{u_{in} d_{h,in}}{\mu / \rho} \tag{4}$$

Where d_h and $d_{h,in}$ are hydraulic diameters in rectangular and cosine ducts respectively.

The Colburn factor j and the Fanning friction factor f are respectively solved as follows [24]:

$$j = \frac{Nu}{Pr^{1/3}.Re} \tag{5}$$

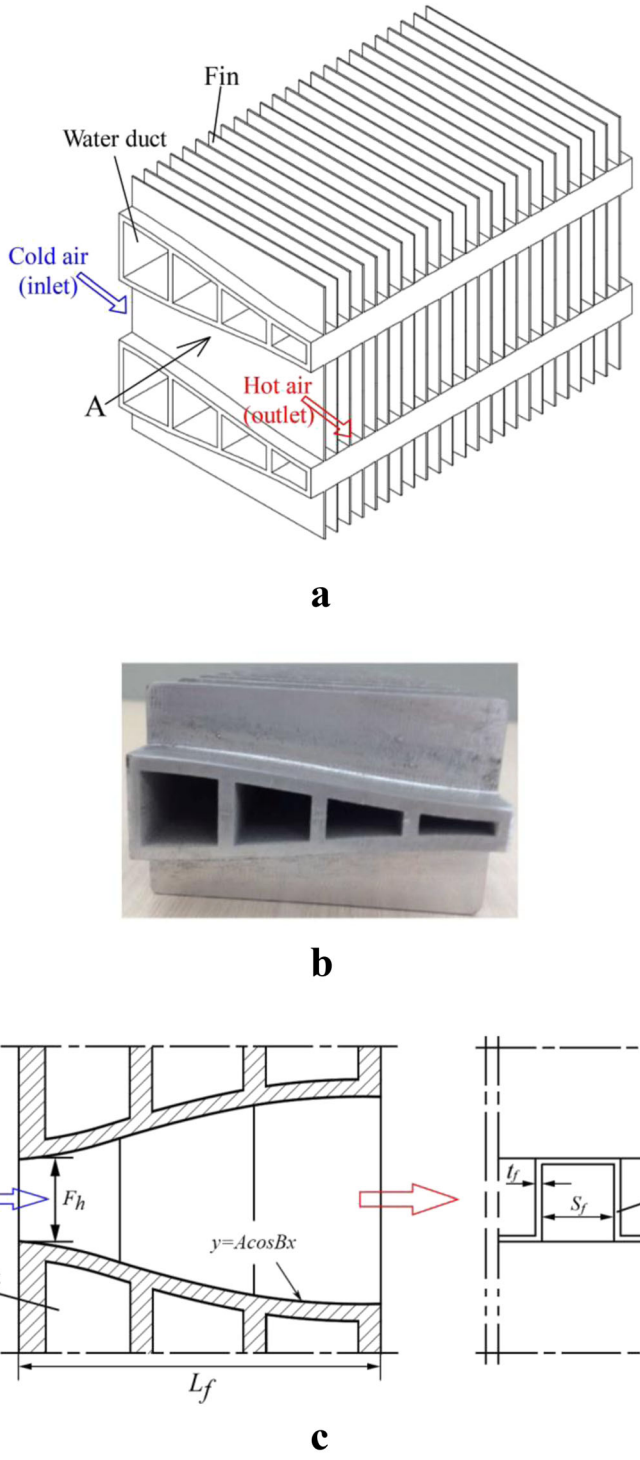

Fig. 1 Cosine style runner. **a** Isometric drawing; **b** The experimental physical drawing (View point A); **c** Schematic diagram of structural parameters (View point A)

$$f = \frac{D_h}{4L_f} \cdot \frac{\Delta p}{(1/2)\rho u^2} \tag{6}$$

Where Re and D_h in the rectangular runner are calculated by using mean velocity (u_m) and hydraulic diameter (d_h) respectively; Re and D_h in the cosine runner are calculated by using maximum velocity (u_{in}) and hydraulic diameter at the inlet ($d_{h,in}$). The difference between d_h and $d_{h,in}$ lie in d_h is hydraulic diameter of rectandular runner with the same form and $d_{h,in}$ is hydraulic diameter at the inlet of the cosine runner.

Table 1 Structural parameters list of cosine style runner

No.	F_h (mm)	2A (mm)	S_f (mm)	L_f (mm)	t_f (mm)
1	9.5	5	4.0	60	0.4
2	10.5	5	4.0	60	0.4
3	11.5	5	4.0	60	0.4
4	9.5	7	4.0	60	0.4
5	10.5	7	4.0	60	0.4
6	11.5	7	4.0	60	0.4
7	9.5	9	4.0	60	0.4
8	10.5	9	4.0	60	0.4
9	11.5	9	4.0	60	0.4

Table 2 Structural parameters list of equal cross section runner

No.	L_f (mm)	S_f (mm)	F_h (mm)	t_f (mm)
1	60	3.0	9.0	0.4
2	60	3.5	9.0	0.4
3	60	4.0	9.0	0.4
4	55	3.0	9.0	0.4
5	55	3.5	9.0	0.4
6	55	4.0	9.0	0.4
7	45	3.0	8.0	0.3
8	45	3.5	8.0	0.3
9	45	4.0	8.0	0.3
10	45	3.0	9.0	0.3
11	45	3.0	11.0	0.3

3 Numerical simulation analysis

3.1 Basic hypothesis and mathematical model

3.1.1 Basic assumption

Before adopting numerical method to analyze the cosine style runner, the following assumptions were made:

(1) The Mach number of air less than 0.3, so air can be considered as incompressible fluid;
(2) The physical model was steady state heat transfer and flow problem.
(3) Ignoring the influence of gravity on numerical results;
(4) Ignoring the effect of radiation heat transfer;
(5) The heat exchange surface was an ideal smooth surface.

3.1.2 Calculation area and boundary conditions

In order to maintain uniform air velocity distribution at the inlet, the computation domain was extended upstream 1.5 times of the flow path length. Also computation domain was

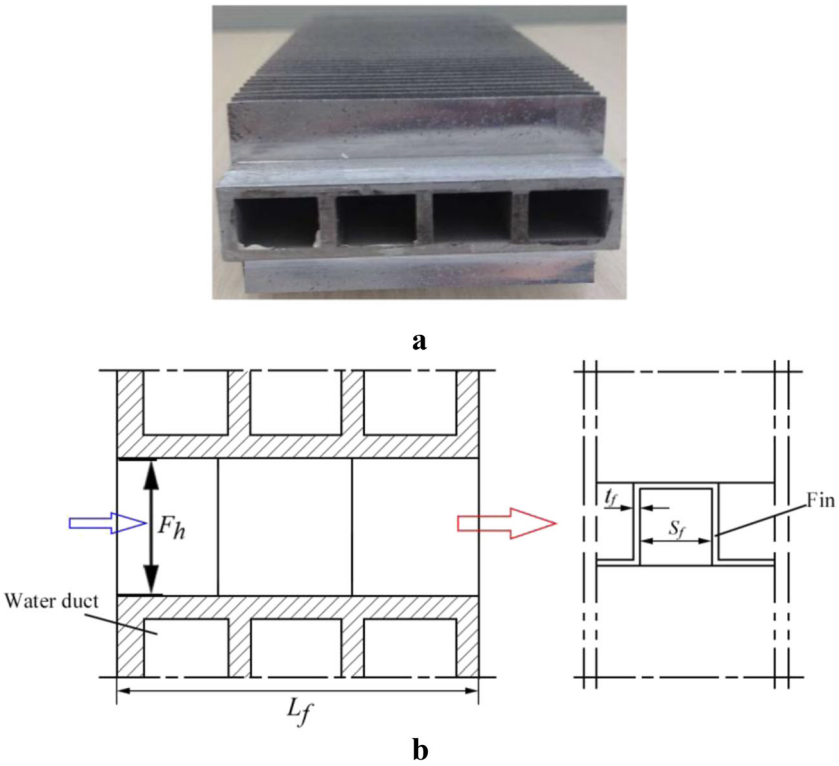

Fig. 2 Equal cross section runner. **a** Picture of real product; **b** Schematic diagram of structural parameters

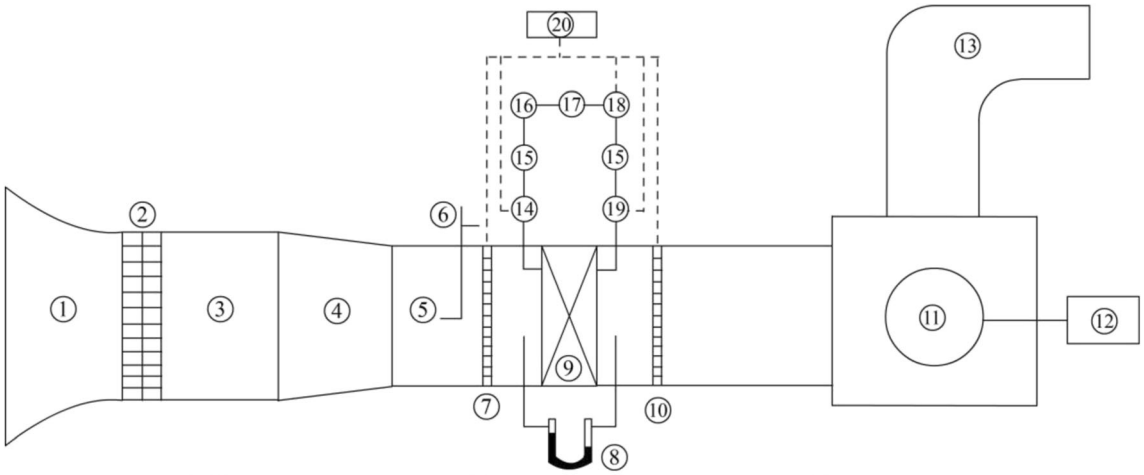

Fig. 3 Schematic diagram of wind tunnel test bed

extended downstream 5 times in order to prevent a backflow phenomenon at the outlet. The boundary conditions employed in the simulation are "velocity-inlet", "pressure-outlet", "symmetry", which is shown in Fig. 4. The model of the heat exchange surface of the cosine style runner was symmetric plane where no heat and mass exchange on it, so the plane can be set as "symmetry" condition. All the wall surfaces except the inlet, the outlet and the symmetrical plane were set as "Wall" conditions, and the heat flow rate on wall surface was set as "0". The initial temperature at the inlet was 293.15 K, and on the fins and cosine surface were 353 K. The static pressure at the outlet is 0 Pa. The air flow rate of the cosine style runner were 0.28, 0.39, 0.5, 0.61, 0.72, 0.83 kg/h respectively.

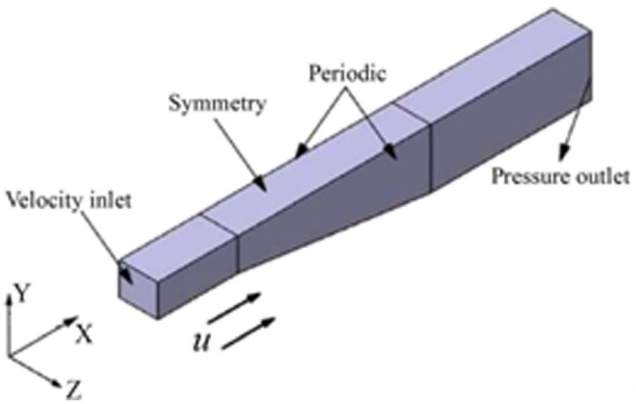

Fig. 4 Three-dimensional calculation model and boundary condition of fin

3.2 Grid division and discretization

The mesh needed to be refined in the vicinity of the wall and fin surfaces in calculation area, and the area was divided by adopting a structured grid partitioning method by using Software ANSYS ICEM. The overall grid structure and the refinement mesh structure near the wall surface are shown in Fig. 5a and b respectively. ANASYS FLUENT software was used as a computing platform to discretize and solve the mass, momentum, energy conservation equations and other control

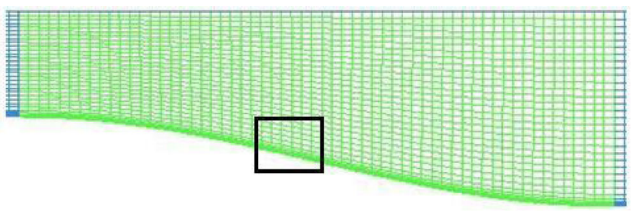

(a) Overall grid

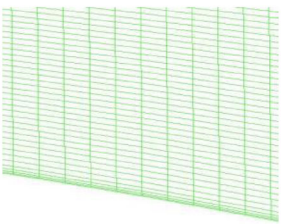

(b)a Local grid

Fig. 5 Cosine runner grid division. **a** Overall grid; **b** Local grid

equations. In this paper, the SIMPLE method was adopted for the velocity and pressure coupling equations, and the momentum, energy and turbulence equations were solved by the second-order windward format. Residual and energy residuals for continuity, velocity components, turbulent kinetic energy, turbulent dissipation, and energy residuals were controlled within 10^{-6}.

3.3 Control equation

In this paper, the RNG k-ε model modified in turbulent state was used to solve the calculation region. The three control equations were as follows:

Continuity equation:

$$\frac{\partial}{\partial x_j}\left(\rho u_j\right) = 0 \tag{7}$$

Momentum equation:

$$\frac{\partial}{\partial x_i}\left(\rho u_i u_k\right) = \frac{\partial}{\partial x_i}\left(\mu \frac{\partial u_k}{\partial x_i}\right) - \frac{\partial p}{\partial x_k} \tag{8}$$

The energy equation is:

$$\frac{\partial}{\partial x_j}\left(\rho u_j T\right) = \frac{\partial}{\partial x_j}\left(\frac{\lambda}{c_p} \cdot \frac{\partial T}{\partial x_j}\right) \tag{9}$$

3.4 Grid independence and mathematical model verification

3.4.1 Grid independence

In the case of a heat exchanger unit, $t_f = 0.4$ mm, $L_f = 60$ mm, $F_h = 10$ mm, $S_f = 4$ mm, $2A = 5$ mm, the independence verification of the grid was carried out with $Re = 3140$. The number of seven different grids was studied, which are 246,000, 400,000, 546,000, 699,000, 852,000, 997,000, 110,100 grids respectively. As shown in Fig. 6, when the number of grids was divided into 997,000 and 1.101 million, the difference between the heat transfer coefficient and the pressure drop of the two calculation models was less than 0.6%. Synthesizes convergence time, convergence precision and economy, the grid number of 997,000 can meet the simulation needs.

3.4.2 Mathematical model verification

Taking $t_f = 0.4$ mm, $L_f = 60$ mm, $F_h = 10$ mm, $S_f = 4$ mm and $2A = 5$ mm of cosine style runner as an example, the numerical solution was carried out under the condition of $500 \leq Re \leq 5000$. In order to verify the simulation method used in this paper, the simulation data was compared with the experimental data of the cosine duct, as shown in Fig. 7a and b. The numerical calculation of j and f factors and the curve of experimental results had good agreement and consistency. Therefore, it was proved that the mathematical model and calculation method used in this paper had certain accuracy and reliability.

4 Results and discussion

4.1 Experimental study on effect of different structural parameters on heat transfer and fluidity

4.1.1 Heat transfer and pressure drop performance

Figure 8 is the relationship between convective heat transfer coefficient and pressure drop of a cosine style runner at different inlet heights F_h (9.5, 10.5 and 11.5 mm) and different amplitudes $2A$ (5, 7 and 9 mm).

We can see that with the increase of air velocity, both h and ΔP increase. In addition, the trend of heat transfer coefficient increases gradually, while the pressure drop is increased in the form of parabolic growth. # 1 and # 9 have maximum and minimum convective heat transfer coefficients, respectively; While # 2 and # 8 have the maximum and minimum pressure drop respectively. By making comparison among # 1, # 2, and # 3, the convective heat transfer performance is increased as the inlet height decreases, that is, the smaller the inlet height the better the convective heat transfer performance. By making comparison among # 2, # 5, and # 8, the convective heat transfer performance is gradually reduced as the amplitude increases, that is, larger amplitude weakens the convective heat transfer performance.

Through multiple regression analysis and F significance test of experimental data, the experimental correlation formulas of j factor and f factor in cosine style runner are obtained, as shown in Eqs. (10) and (11) respectively.

The relative accurate prediction of j and f factors can be accomplished by two test correlations, and the predictive error of 90% of the experimental data is within ±10%. Comparing with the experimental values, the arithmetic mean error between j factor and f factor are 0.35 and 4.1%, and the mean deviation are 2.5 and 4.9%, respectively.

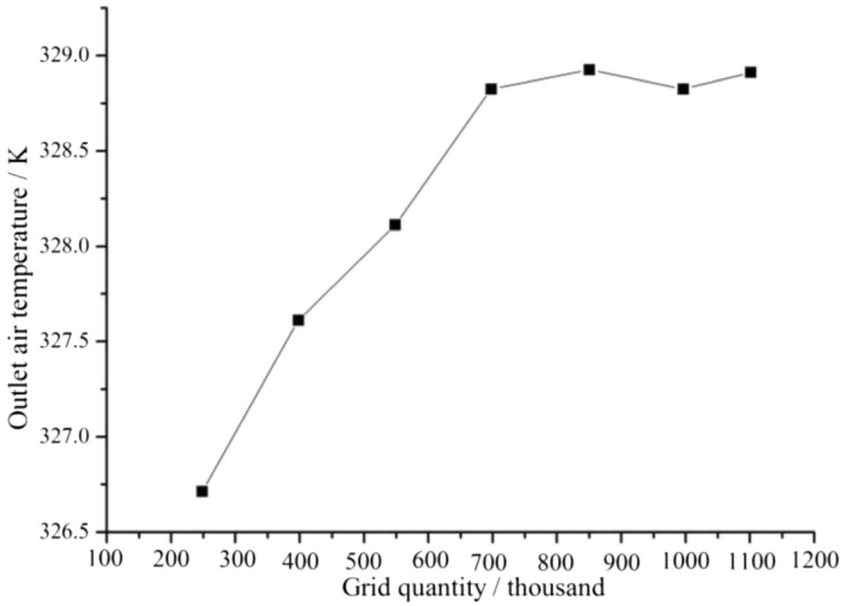

Fig. 6 Grid independence verification

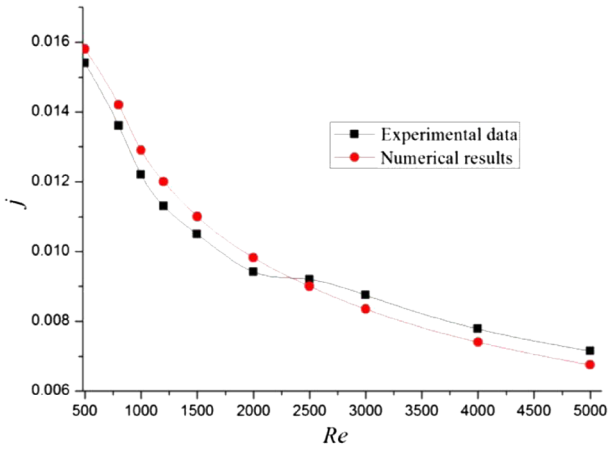

(a) *j*factor

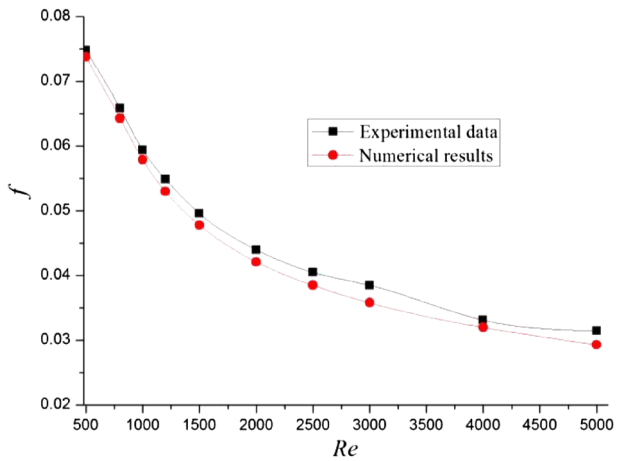

(b) *f* factor

Fig. 7 Comparison of simulation values and experimental data. **a** *j* factor; **b** *f* factor

$$j = 0.1136Re^{-0.199}\left(S_f/F_h\right)^{0.229}\left(S_f/2A\right)^{-0.143}\left(L_f/t_f\right)^{-0.426} \tag{10}$$

$$f = 1.48Re^{-0.25}\left(S_f/F_h\right)^{0.527}\left(S_f/2A\right)^{-0.215}\left(L_f/t_f\right)^{-0.243} \tag{11}$$

4.1.2 Contrast analysis of integrated heat transfer performance of cosine and equal cross section flow path

The Core Volume Goodness Factor is used to evaluate the overall heat transfer performance of the two different ducts including cosine style runner and equal cross section runner. The significance of using the Core Volume Goodness Factor is that it can compare the overall heat transfer performance of different ducts with different structures. The Core Volume Goodness Factor was proposed by Shah and Sekulić [25] and its expression is

$$\eta_o h_{std}\alpha = \frac{c_p\mu}{Pr^{2/3}}\eta_o\frac{4\sigma}{D_h^2}jRe \tag{12}$$

$$E_{std}\alpha = \frac{\mu^3}{2g_c\rho^2}\frac{4\sigma}{D_h^4}fRe^3 \tag{13}$$

In the above equation, $\eta_o h_{std}\alpha$ is energy consumption per unit volume while the temperature changes by 1 K in a heat exchanger; $E_{std}\alpha$ is the frictional power consumed per unit volume. The subscript "*std*" is arbitrarily selected standard temperature and pressure conditions. From the perspective of the volume of the heat exchanger, in the case of the same $E_{std}\alpha$, the larger the $\eta_o h_{std}\alpha$, the smaller the volume of the heat exchanger used at the same heat transfer capacity. That is, with

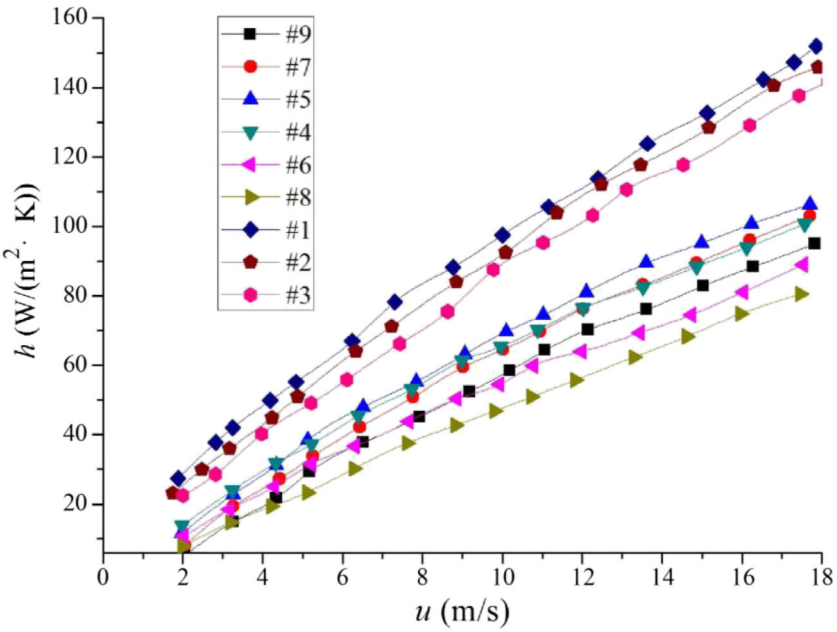

(a) Heat transfer performance comparison

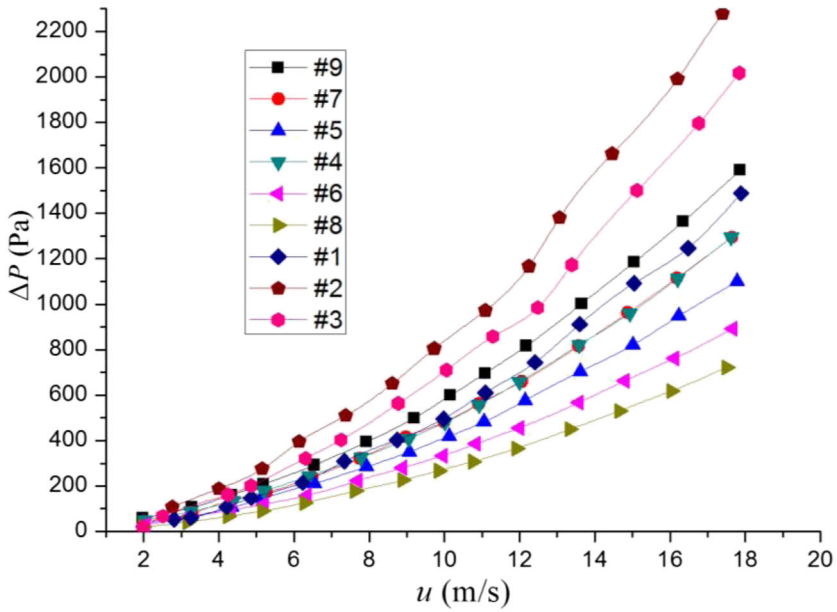

(b) Resistance performance comparison

Fig. 8 Analysis of performance in different Cosine runners. **a** Heat transfer performance comparison; **b** Pressure drop performance comparison

the same "$E_{std}\alpha$", a larger value of $\eta_o h_{std}\alpha$ means that only a small heat exchanger volume is required at the same heat capacity. Re_m is the mean Reynolds number calculated in the rectangular runner; Re_{max} is the maximum Reynolds number calculated in the cosine runner at the inlet ($d_{h,in}$).

The variation curve of "$\eta_o h_{std}\alpha$" value with "$E_{std}\alpha$" is given in Fig. 9. As can be seen from the figure, the "$\eta_o h_{std}\alpha$" values for both structures are increased as the "$E_{std}\alpha$" increases. From the results of the comparative analysis, under the same "$E_{std}\alpha$", the cosine style runner has the best comprehensive enhanced heat transfer effect. In the whole $E_{std}\alpha$ interval, the $\eta_o h_{std}\alpha$ value in the cosine style runner is about 7–25% greater than the $\eta_o h_{std}\alpha$ value in the equal cross section runner. The value of $\eta_o h_{std}\alpha$ for the cosine style runner is about 25% greater than that of equal cross section runner when $E_{std}\alpha$ is the largest. Therefore, the overall heat transfer

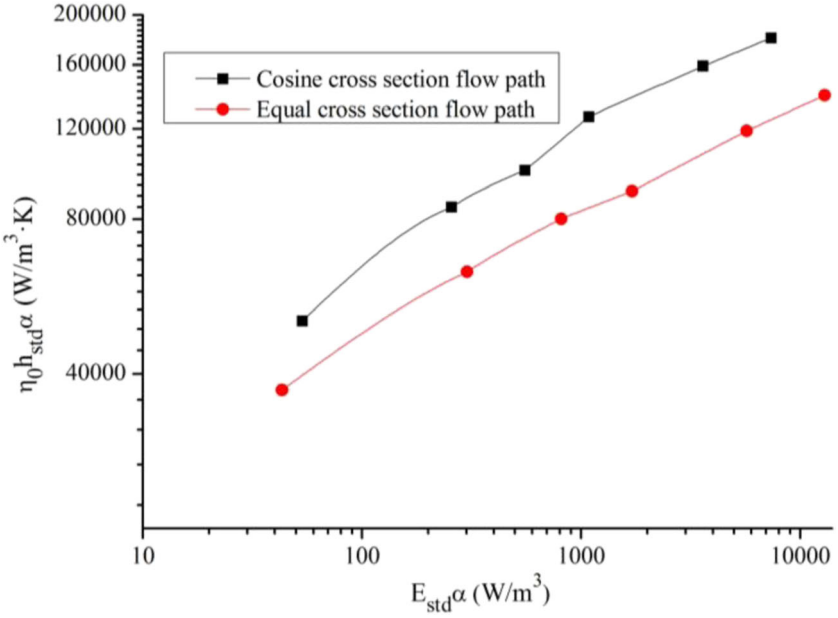

Fig. 9 Comparison of core volume goodness factors under different special-shaped runner structures

performance of the cosine style runner mentioned in this paper is better than that of the equal cross section runner.

4.2 Effect of amplitude on heat transfer and resistance performance

Figure 10 shows the j and f factors of the cosine style runners with different amplitudes. The runners have the same L_f (53 mm), S_f (2.5 mm) and F_h (8.0 mm), but have different amplitudes. As can be seen from the figure, the j factor and the f factor decrease with the increase of Re. With the same Re, the increment of j and f factors is substantially consistent. That is to say, the increase of amplitude does not result in dramatic changes of the j factor and f factor. Under the same Re, the j factor and f factor increase as the amplitude decreases. So the small amplitude plays an important role in heat transfer, but the small amplitude also brings a relatively large pressure drop. And the amplitude $2A = 5$ mm has the best j factor and the maximum f factor. When $1210 \le Re \le 5080$, the j factors of the runners with amplitude $2A = 7$ mm and $2A = 9$ mm were reduced by 6.96 and 12.6% respectively. Meanwhile, the f factors decreased by 29.8 and 50% respectively.

In this paper, the influence of j factor and f factor must be comprehensively considered. JF factor is used as an evaluation index for the comprehensive enhanced heat transfer performance.

The expression of the JF factor is [26]:

$$JF = \frac{j_i/j_0}{(f_i/f_0)^{1/3}} \tag{14}$$

Where the subscript "i" represents different runners and the "0" represents a reference runner with equal cross sections.

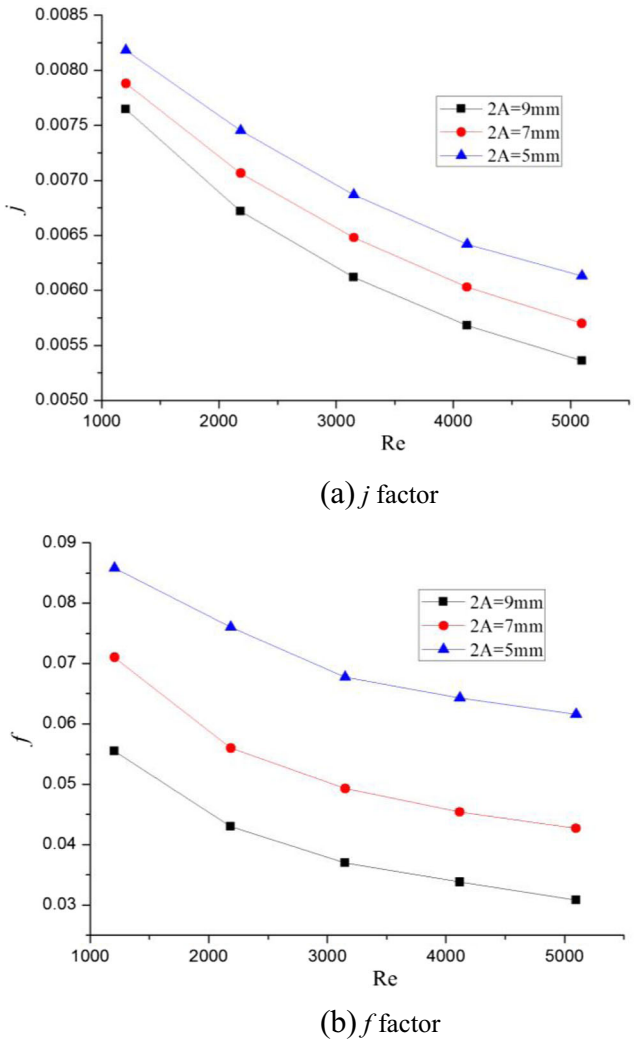

Fig. 10 Comparison of heat transfer and resistance performance of different amplitude. **a** j factor; **b** f factor

The higher the *JF* factor is, the better thermal performance is.

In Fig. 11, the effect of the *JF* factor on the comprehensive enhanced heat transfer in three different cosine style runners is compared. As can be seen from the figure, with the same Re, the flow path of amplitude $2A = 5$ mm has the largest *JF* factor value. That is, the smaller the amplitude, the better the heat transfer performance of the cosine runner.

4.3 Temperature field and flow field with different amplitudes

Taking the case of $Re = 3140$ as an example, the cosine style runners with amplitude of 5, 7 and 9 mm were numerically analyzed. Figure 12a and b are distribution images of the temperature field and velocity field under different amplitudes respectively, and the cloud picture section is the middle plane of two adjacent fins.

The temperature field images corresponding to different amplitudes are shown in Fig. 12a. For three different amplitudes, the temperature in the mainstream region near the intermediate fluid domain is relatively low and the temperature value near the wall surface is relatively high. Therefore, the process of convection heat transfer mainly depends on the convection and heat conduction of the wall surface or fin surface. The comparison of the three sub-graphs in the figure shows that the thermal boundary layer thickness gradually increases as the amplitude increases from 5 to 9 mm. This explains the larger the amplitude, the thicker the thickness of the thermal boundary layer, and the weaker the heat transfer performance.

The velocity field images corresponding to different amplitudes are shown in Fig. 12b. It can be seen from the figure that the flow rate of the main stream is relatively high and the flow rate near the wall is relatively low. This is because the air is affected by the effect of the viscous force on the wall when the air flows through the wall. In addition, the thickness of the velocity boundary layer is gradually thickened as the amplitude increases. With the increase of the amplitude, there has no backflow or boundary layer separation in the flow domain. It is because the maximum slope angle in the domain does not reach the degree of boundary layer separation. As the amplitude decreases, the high speed region of the intermediate fluid region is pushed forward. This indicates that the smaller amplitude has better heat transfer performance.

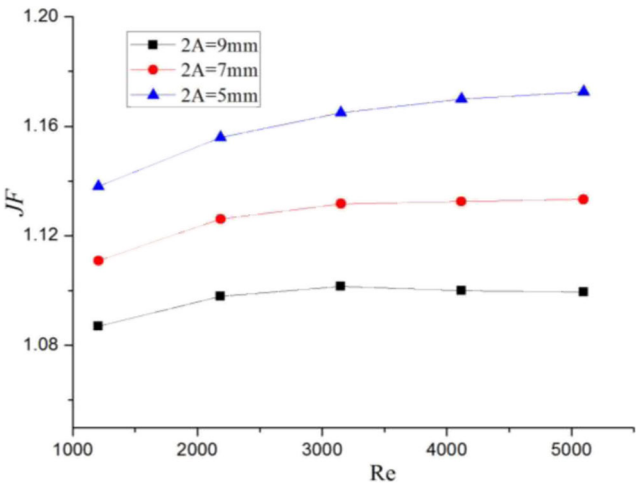

Fig. 11 Comparison of enhanced heat transfer effects of three different amplitudes

4.4 Temperature field and velocity field with different Reynolds numbers

The cosine style runner are numerically analyzed when Reynolds numbers are 1210, 2170, 3140, 4110 and 5080. Figure 13a and b are distribution images of the temperature field and velocity field under different *Re* conditions respectively.

The selected plane for exhibition is the middle position of two adjacent fins. The temperature field contours corresponding to different Reynolds number are shown in Fig. 13a. As can be seen from the figure, for the five different Reynolds numbers, the temperature in the main flow zone near the intermediate fluid domain is relatively low, and the temperature near the wall surface is higher. Therefore, in the cosine style runner, heat transfer near the wall surface plays a leading role. Comparing the five subgraphs in the figure, it can be found that the thickness of the thermal boundary layer gradually decreases during the increase of Reynolds number. This means that the larger the Reynolds number, the smaller the thickness of the thermal boundary layer and the stronger the heat transfer performance. Therefore, the greater the Re is, the stronger the convective heat exchange enhancement.

As shown in Fig. 13b, a velocity field cloud image corresponding to different *Re* is displayed. Wherein red represents high speed region, blue represents low speed region. It can be seen from the figure that the flow rate in the main stream is relatively high but the flow rate near the wall is relatively lower with different *Re*. This is because the air is affected by the effect of the viscous force on the wall when the air flows through the wall. In addition, there is also a velocity boundary layer at the proximal wall. By contrast of the five sub-graphs in the graph, it is found that the thickness of the velocity boundary layer is gradually reduced as *Re* increases. Another significant phenomenon that can be found from velocity field clouds is that with the increase of *Re*, the high speed region of the intermediate fluid region is pushed forward. The higher velocity in the runner also increases convective heat transfer performance.

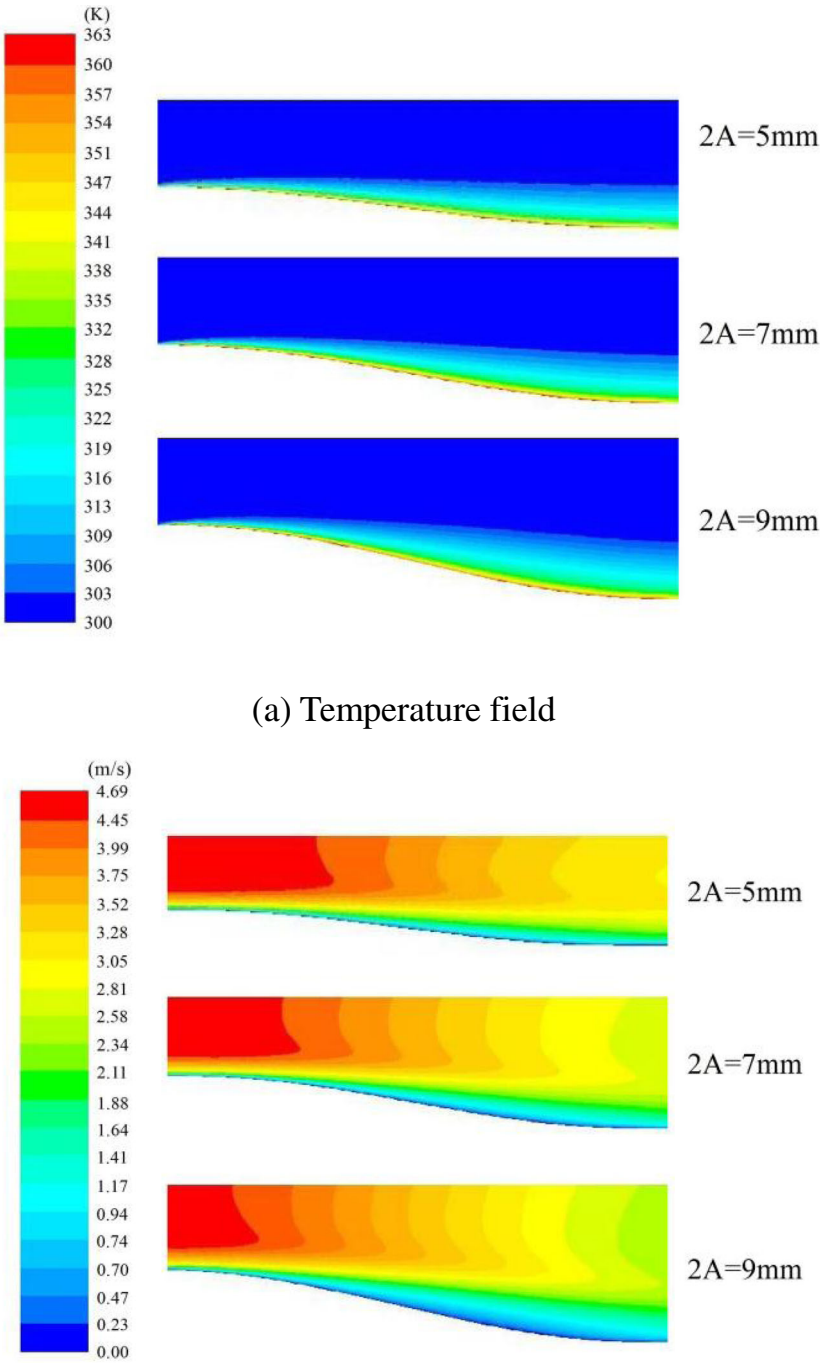

Fig. 12 Effect of different amplitude on temperature field and velocity field. **a** Temperature field; **b** Velocity field

4.5 Strengthening heat transfer mechanism of cosine style runner based on field synergy theory

The field synergy theory is mainly to determine the synergy between the temperature field and the velocity field by calculating the angle between the velocity vector and the temperature gradient. The field synergy can be evaluated by local field synergy angle and average field synergy angle. The smaller the average field synergy angle, the more favorable the heat transfer is facilitated. The relationship between velocity vector and temperature gradient, local field synergy angle θ' and the average field synergy angle (FSA) θ is defined as follows [27]:

$$\overrightarrow{U}\cdot\nabla T = |\overrightarrow{U}|\cdot|gradT|cos\theta' \tag{15}$$

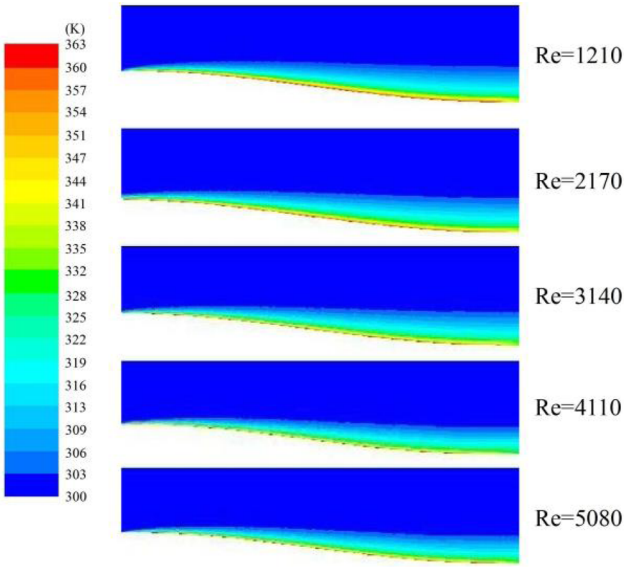

(a) Temperature field

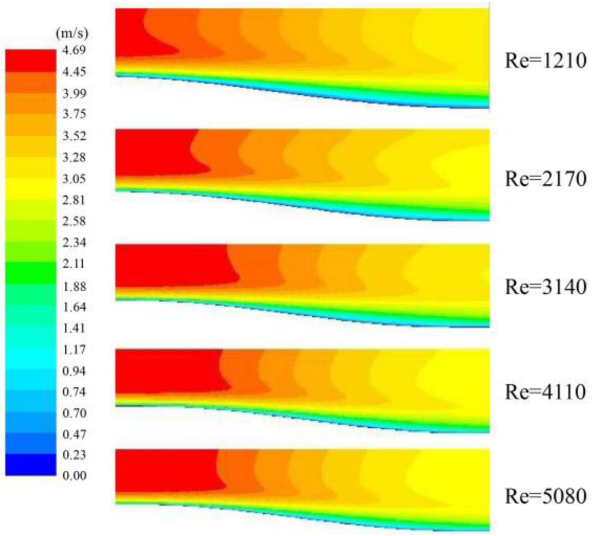

(b) Velocity field

Fig. 13 Effect of different *Re* on temperature field and velocity field. **a** Temperature field; **b** Velocity field

$$\theta' = cos^{-1}\frac{u\frac{\partial T}{\partial x} + v\frac{\partial T}{\partial y} + w\frac{\partial T}{\partial z}}{|\vec{U}|\cdot|gradT|} \tag{16}$$

$$\theta = \frac{\int \theta' dV}{\int dV} \tag{17}$$

In above equations, u, v, w are represented velocities in x, y, z coordinate axes, $\vec{U}$ is the velocity vector, ∇T is the temperature gradient, and V is the minute control body in the discretized fluid region.

Figure 14 shows a local field synergy profile under the same inlet air flow rate $u = 4$ m/s ($Re = 3140$). It can be seen from the figure that there is a certain similarity to the distribution of the local field synergy angles in the cosine style runners of three different amplitudes. The local field synergy angle distribution in the cosine runner and the equal cross section runner is different. The inner wall of the equal cross section runner has a small local field synergy angle because the wall surface or the fin surface has large temperature gradient and velocity gradient [28]. A large local field synergy in the cosine style flow path occurs at the wall surface, while the smaller local field synergy is mainly distributed in the inlet and the central main region. When the amplitude is 5 mm, the field synergy angle distribution at the center region is good. However, the field synergy angle inside the central region is mixed with larger field synergy angle when the amplitude is 7 and 9 mm. Therefore, the magnitude of amplitude has a certain effect on the degree of field synergy.

Figure 15 shows a plot of the average field synergy with different *Re* numbers and different amplitudes. As can be seen from the figure, under the same *Re* condition, with the increase of the amplitude, the average field synergy is increased, which is not conducive to enhanced heat transfer. Therefore, the smaller the amplitude is, the smaller the average field synergy angle, the better the field synergy. When $Re > 3000$, the average field synergy angle of three different amplitudes is increased with a smaller amplitude. But when $Re < 3000$, the average field synergy angle of three different amplitudes is increased with a larger amplitude. Therefore, increasing the Reynolds number to a certain extent does not have a great influence on the average field synergy.

5 Conclusions

This paper presents the steady state heat transfer and friction characteristics and performance analysis of convective heat transfer through a cosine style runner with different amplitudes 2A (5, 7 and 9 mm). We concluded that:

(1) At the same amplitude, the convective heat transfer performance gradually increases as the inlet height (F_h) decreases. At the same inlet height (F_h), the convective heat transfer performance is gradually reduced as the amplitude increases, that is, the larger amplitude weakens the convective heat transfer performance.
(2) Through the regression analysis method and the F significance test method, the experimental data of heat transfer and resistance performance of various structures is fitted, and the obtained j and f factors correlation formula can predict 90% data, and the error range is within ±10%.

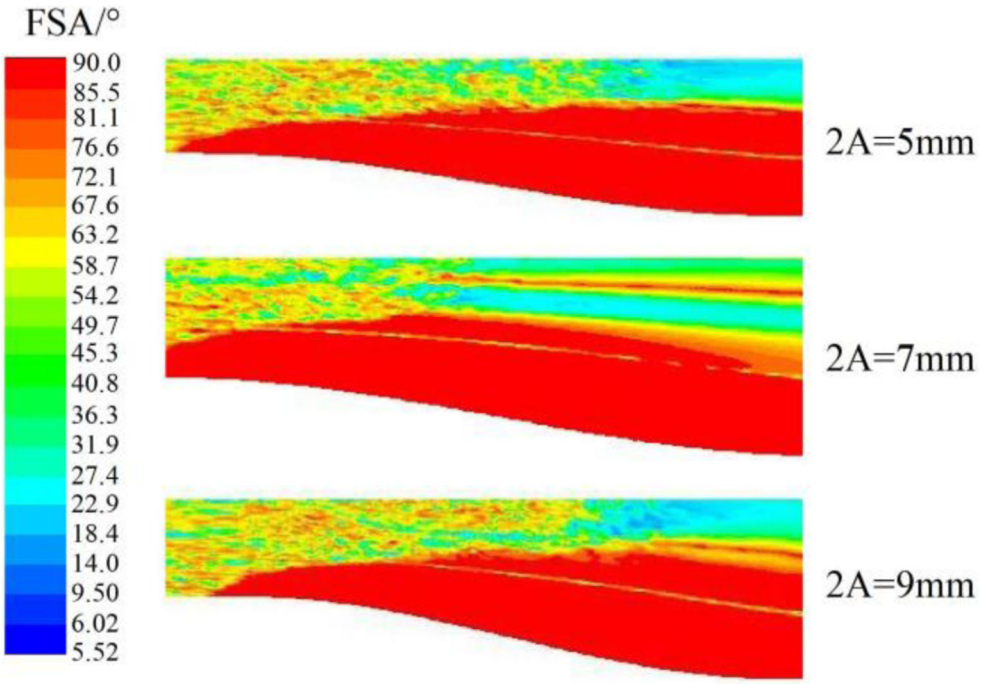

Fig. 14 Local field synergy angle distribution

(3) In the range of 5 mm ≤ 2*A* ≤ 9 mm, with the decrease of amplitude, the overall heat transfer performance is better and the cosine style runner at 2*A* = 5 mm has the largest *JF* factor. At the same amplitude, the thickness of the thermal boundary layer and velocity boundary layer is decreasing as the Reynolds number increases. Under the same *Re* condition, with the decrease of amplitude, the average field gradually decreases, and therefore, the smaller amplitude has a better field synergy.

(4) In the cosine style runner of 5 mm ≤ 2*A* ≤ 9 mm, with the decrease of amplitude, the smaller the average field synergy angle (*FSA*), the better the field synergy. When compared with the runner structure of 2*A* = 5 mm, the *j* factors of 7 and 9 mm decreased by 6.96 and 12.6% respectively, and the *f* factors decreased by 29.8 and 50% respectively. That is, the small amplitude increases the pressure drop while facilitating heat transfer. And with the increase of amplitude, the thickness of the boundary layer increases gradually.

(5) By using the Core Volume Goodness Factor to compare the overall enhanced heat transfer performance of the cosine and other equal cross section runners, it is concluded that the value of $\eta_o h_{std}\alpha$ in the cosine style runner is 25% larger than that of the equal cross section runner, and the heat transfer performance of the cosine type runner structure is greatly improved.

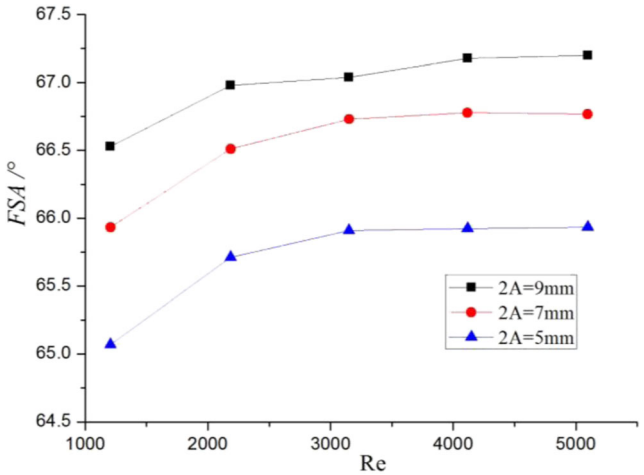

Fig. 15 Comparison of average field synergy at different amplitudes

Acknowledgements Financial support is provided by the National Science Foundation of China (51874187, 51806114), China Postdoctoral Fund (2016 M602170, 2017 T100508), Key research and development plan of Shandong Province (2017GSF20113, 2018GSF121002), Shandong Province Natural Science Foundation (ZR2018MEE002, ZR2017PD011).

References

1. Liu JC, Wei XT, Zhou ZY, Wei ZW (2018) Numerical analysis on interactions between fluid flow and structure deformation in plate-fin heat exchanger by Galerkin method. Heat Mass Transf 55: 2835–2844
2. Kuehndel J, Kerler B, Karcher C (2018) Selective laser melting in heat exchanger development-experimental investigation of heat transfer and pressure drop characteristics of wavy fins. Heat Mass Transf 54:2187–2193
3. Wu HY, Cheng P (2003) Friction factors in smooth trapezoidal silicon microchannels with different aspect ratios. Int J Heat Mass Transf 46:2519–2525

4. Kuo JK, Yen TS, Chen CK (2008) Improvement of performance of gas flow channel in PEM fuel cells. Energy Convers Manag 49: 2776–2787
5. Amirahmadi S, Rashidi S, Esfahani JA (2016) Minimization of exergy losses in a trapezoidal duct with turbulator roughness and beveled corners. Appl Therm Eng 107:533–543
6. Farhanieh B, Sunden B (1991) Three-dimensional laminar flow and heat transfer in the entrance region of trapezoidal ducts. Int J Numer Methods Fluids 13:537–559
7. Li Y, Deng H, Tao Z, Xu G, Chen Y (2017) Heat transfer characteristics in a rotating trailing edge internal cooling channel with two coolant inlets. Int J Heat Mass Transf 105:220–229
8. Cur NO, Anselmino JJ (1992) Evaporator for home refrigerator, US Patent 5, 157, 941
9. Waltrich PJ, Barbosa JR, Melo C, Hermes CL (2008) Air-side heat transfer and pressure drop in accelerated flow evaporators. Int. Refrig. Air Cond. Conference, vol 7, pp 2311–2319
10. Waltrich PJ, Barbosa JR, Hermes CL (2011) COP-based optimization of accelerated flow evaporators for household refrigeration applications. Appl Therm Eng 31:129–135
11. Waltrich PJ, Barbosa JR, Hermes CL, Melo C (2011) Air-side heat transfer and pressure drop characteristics of accelerated flow evaporators. Int J Refrig 34:484–497
12. Rush TA, Newell TA, Jacobi AM (1999) An experimental study of flow and heat transfer in sinusoidal wavy passages. Int J Heat Mass Transf 42:1541–1553
13. Akbarzadeh M, Rashidi S, Bovand M, Ellahi R (2016) A sensitivity analysis on thermal and pumping power for the flow of nanofluid inside a wavy channel. J Mol Liq 220:1–13
14. Lu S, Li L, Cheng Y, Sa Z, Zhang Y (2017) Mechanical failure mechanisms and forms of normal and deformed coal combination containing gas: model development and analysis. Eng Fail Anal 80: 241–252
15. Fan T, Zhou G, Wang J (2018) Preparation and characterization of a wetting – agglomeration - based hybrid coal dust suppressant. Process Saf Environ Prot 113:282–291
16. Zhou G, Zhang Q, Bai R, Fan T, Wang G (2017) The diffusion behavior law of respirable dust at fully mechanized caving face in coal mine: CFD numerical simulation and engineering application. Process Saf Environ Prot 106:117–128
17. Abhishek RG, Arun KS (2016) Numerical study of fully developed unsteady flow and heat transfer in asymmetric wavy channels. Int J Heat Mass Transf 102:98–112
18. Bahaidarah HM (2016) Entropy generation during fluid flow in sharp edge wavy channels with horizontal pitch. Adv Mech Eng 8:1–10
19. Akbarzadeh M, Rashidi S, Esfahani JA (2017) Influences of corrugation profiles on entropy generation, heat transfer, pressure drop, and performance in a wavy channel. Appl Therm Eng 116:278–291
20. Sarkar M, Paramane SB, Sharma A (2016) Periodically fully developed heat and fluid flow characteristics in furrowed wavy channel. Heat Transfer Eng 38:278–288
21. Zhu D, Xu H, Sun Y, Qi B (2010) Numerical heat transfer analysis of laminar film condensation on a vertical fluted tube. Appl Therm Eng 30:1159–1163
22. Mofft RJ (1988) Describing the uncertainties in experiment results. Exp Thermal Fluid Sci 1:3–17
23. Zhang X, Wang Y, Cang P, Wang R (2016) Experimental investigation of thermal hydraulic performance of heat exchangers with different Reynolds numbers on both air-side and water-side. Appl Therm Eng 99:1331–1339
24. Ismail LS, Velraj R (2009) Studies on fanning friction (f) and Colburn (j) factors of offset and wavy fins compact plate fin heat exchanger – a CFD approach. Numer Heat Trans A-Appl 56:987–1005
25. Shah RK, Sekulić DP (2003) Fundamentals of heat exchanger design. Wiley, New Jersey
26. Yakut K, Alemdaroglu N, Kotcioglu I, Celik C (2006) Experimental investigation of thermal resistance of a heat sink with hexagonal fins. Appl Therm Eng 26:2262–2271
27. Zhang X, Wang Y, Yu Z, Zhao D (2015) Numerical analysis of thermal-hydraulic characteristics on serrated fins with different attack angles and wavelength to fin length ratio. Appl Therm Eng 91: 126–137
28. Li J, Peng H, Ling X (2013) Numerical study and experiemental verification of transverse direction type serrated fins and field synergy principle analysis. Appl Therm Eng 54:328–335